Biophysical Journal, Volume *116*

Supplemental Information

Site-Specific Peptide Probes Detect Buried Water in a Lipid Membrane

Jennifer C. Flanagan and Carlos R. Baiz

SUPPORTING INFORMATION

Site-specific peptide probes detect buried water in a lipid membrane

Jennifer C. Flanagan[1] and Carlos R. Baiz[1,*]

[1]*Department of Chemistry, University of Texas at Austin*

*cbaiz@cm.utexas.edu

S1. Sample Preparation

a. Isotope site selection

Prior to selecting sites for isotope incorporation, representative FTIR spectra of helical pHLIP in DMPC bilayers were generated using the MD simulation and electrostatic map procedure described in Section S5 below. Isotope spectra were generated from the same trajectory applying a -60cm^{-1} shift to the residue of interest. Using the simulated spectra as a guide, we selected four sites displaying isotope peaks that were strong, narrow, and fully resolved from the main band. In addition, sites were selected such that they were located in different regions of the membrane system. A13 is located within the hydrophobic region of the lipid tails; L24 is primarily within the hydrophobic lipid tails but accessible to water; L28 lies at the lipid-water interface; and A32 is fully solvated, according to simulations. The calculated spectra for these four sites are given in **Figure S1**.

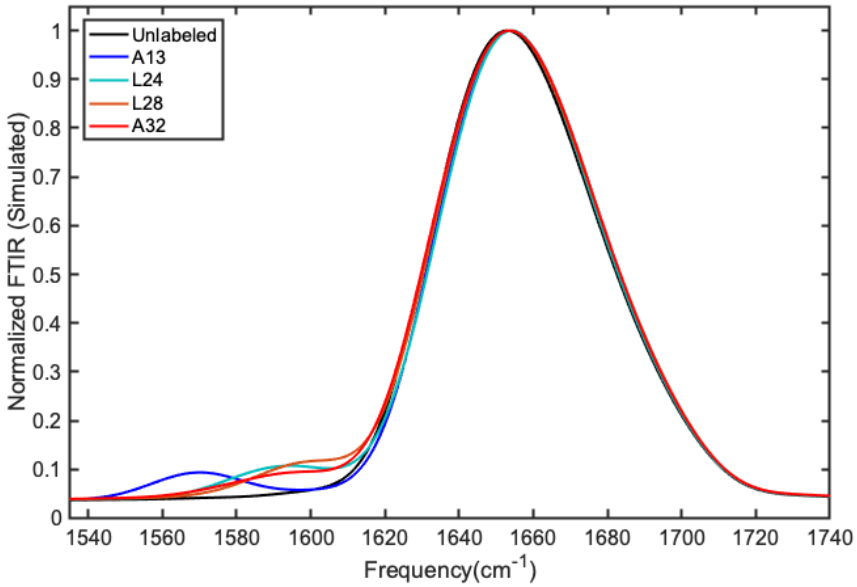

Figure S1. *Calculated IR absorption spectra of the selected isotope label sites.*

b. Isotope label synthesis

N-(9-Fluoroenylmethoxycarbonyl)-L-alanine-1-^{13}C (Fmoc-Ala-OH-1-^{13}C) and N-(9-Fluoroenylmethoxycarbonyl)-L-leucine-1-^{13}C (Fmoc-Ala-OH-1-^{13}C) were purchased from Sigma-Aldrich and used without further purification. $H_2{}^{18}O$ was purchased from Isoflex USA. Prior to use, a 50-mL round bottom flask equipped with a condenser column was assembled and heated to 115 °C for 15 minutes then cooled under nitrogen gas to ensure no water was present. One gram of the ^{13}C enriched amino acid was added to the round bottom flask and dissolved in 1mL ^{18}O water using 1,4-dioxane as a cosolvent in a 4:1 dioxane:water ratio. Acetyl chloride was slowly added to a final concentration of 1M in $H_2{}^{18}O$. The setup was purged with pure nitrogen gas for 15 minutes, then heated to 100 °C and refluxed for 48 hours. Products were recovered via

lyophilization of remaining solvent and characterized by mass spectrometry. The lyophilized powder was dissolved in 20% acetonitrile in water and analyzed with flow injection analysis electrospray ionization mass spectrometry (FIA-ESI-MS) in both positive and negative ion modes to ensure ~85% enrichment. No further purification steps were required following MS analysis. The isotope-enriched FMOC-protected amino acids were sent to Biosynthesis, Inc. (Lewisville, TX) and used in solid-state peptide synthesis of singly labeled pHLIPs. pHLIP sequence is AAEQNPIYWARYADWLFTTPLLLLDLALLVDADEGT. Termini are NH_3 and COO^-, respectively.

c. IR sample preparation

Pure (3-(N-morpholino)propanesulfonic acid) (MOPS) was purchased from Sigma-Aldrich, and was dissolved in D_2O and lyophilized before use to exchange acidic hydrogens for deuterium. Deuterated-MOPS was dissolved in D_2O to a 100 mM concentration, and the pH was adjusted to 8.0 using DCl and NaOD. pHLIP was dissolved in DCl solution (1% v/v in D_2O) and lyophilized to remove remaining TFA counterions from synthesis. This was repeated three times until all TFA had been removed, as confirmed by the absence of the TFA carboxylate peak in the FTIR spectra. DMPC was purchased from Avanti Polar Lipids as 25 mg/mL solution in chloroform. Unilamellar DMPC vesicles were formed by drying DMPC under nitrogen overnight and reconstituting to 30 mM in 100mM MOPS buffer (pH 8.0). Samples were sonicated for 10 minutes then extruded with a 100 nm membrane. A 2 mM pHLIP solution was added to the DMPC solutions to a final peptide concentration of 0.6 mM pHLIP for IR data collection. Each sample was adjusted to a pH of 4 (uncorrected pH reading in D_2O) and incubated for 30 minutes before measurement. Samples and stock solutions were stored frozen at -20 °C prior to the IR measurements.

S2. Sample Characterization

a. Isotope synthesis – MS Results

Synthesis products were provided to the UT-Austin mass spectrometry (MS) facility for characterization. The raw results (**Figure S2** and **Figure S3**) from ESI MS in positive ion mode are below. Results showed the presence of $[M+Na]^+$ adducts corresponding to an unlabeled (^{13}C,2x^{16}O), a singly labeled (^{13}C,^{18}O,^{16}O), and a doubly labeled (^{13}C,2x^{18}O) product for both alanine and leucine. Percent enrichment was taken as the sum of the percent composition of the doubly labeled species plus half of the percent composition of the singly labeled species, with a target of >80% enrichment.

Alanine

Exact mass 316.3 g/mol; $[M+Na]^+$ adduct: 339.1179 m/z

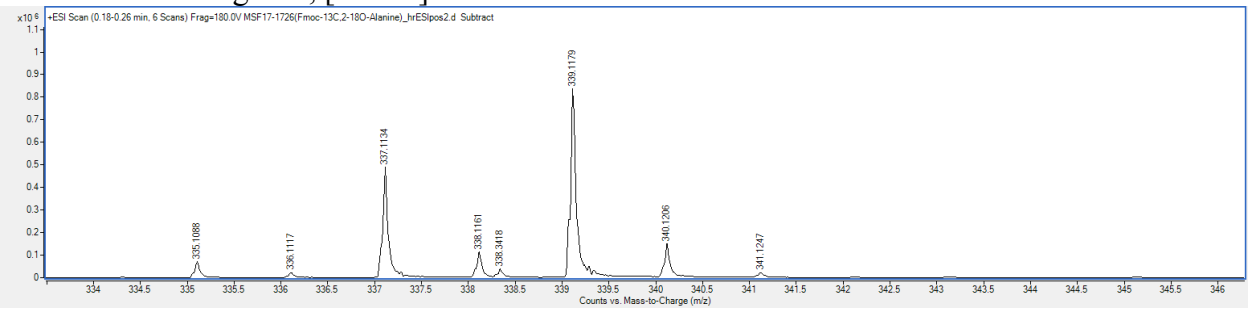

Figure S2. *Mass spectrum including $[M+Na]^+$ adducts obtained from +ESI scan of ^{13}C,^{18}O-Alanine synthesis product, courtesy of UT Austin Mass Spectrometry facility.*

m/z	Species	Abundance	% Composition
335.1084	[^{13}C,2x^{16}O]	21849.36	2.722
337.1130	[^{13}C,^{18}O,^{16}O]	193766.99	24.14
339.1176	[^{13}C,2x^{18}O]	587172.82	73.14

Calculated percent enrichment is 85.21%.

Leucine

Exact mass 358.17 g/mol; $[M+Na]^+$ adduct: 381.163 m/z

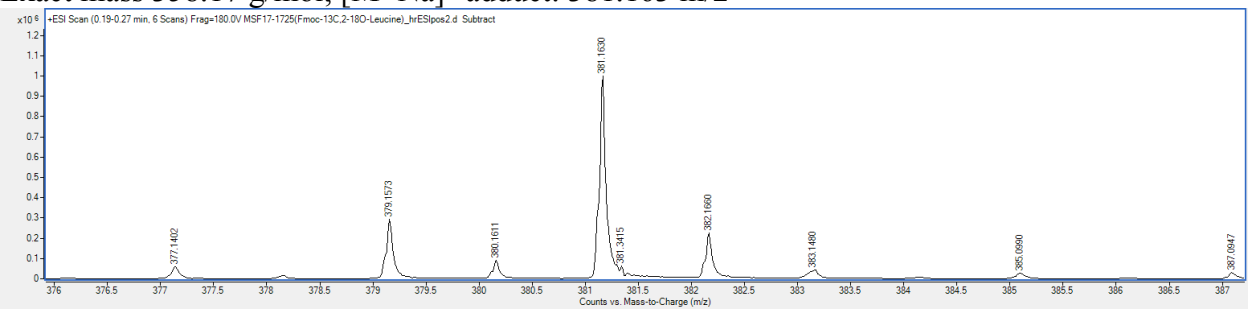

Figure S3. *Mass spectrum including $[M+Na]^+$ adducts obtained from +ESI scan of ^{13}C,^{18}O-Leucine synthesis product, courtesy of UT Austin Mass Spectrometry facility.*

m/z	Species	Abundance	% Composition
377.1402	[^{13}C,2x^{16}O]	58505.67	4.289
379.1563	[^{13}C,^{18}O,^{16}O]	297922.31	21.84
381.1630	[^{13}C,2x^{18}O]	1007579.8	73.87

Calculated percent enrichment is 84.79%.

b. Secondary structure determination – CD Results

Figure S4 shows CD results for pHLIP with DMPC vesicles in MOPS at pH 4 and pH 8. For CD, a 1:30 dilution of the FTIR samples was prepared in 100 mM MOPS buffer for a final peptide concentration of 0.02 mM. CD data was collected from 190 to 300 nm using a 1 mm quartz cuvette. The pH 4 result shows features characteristic of an alpha helix including the combination of a positive band around 193nm and two negative bands around 208nm and 222nm (1). In contrast, these features are absent from the sample held at pH 8, which also shows low ellipticity beyond 210nm. Both of these factors are characteristic of disordered proteins and peptides (2).

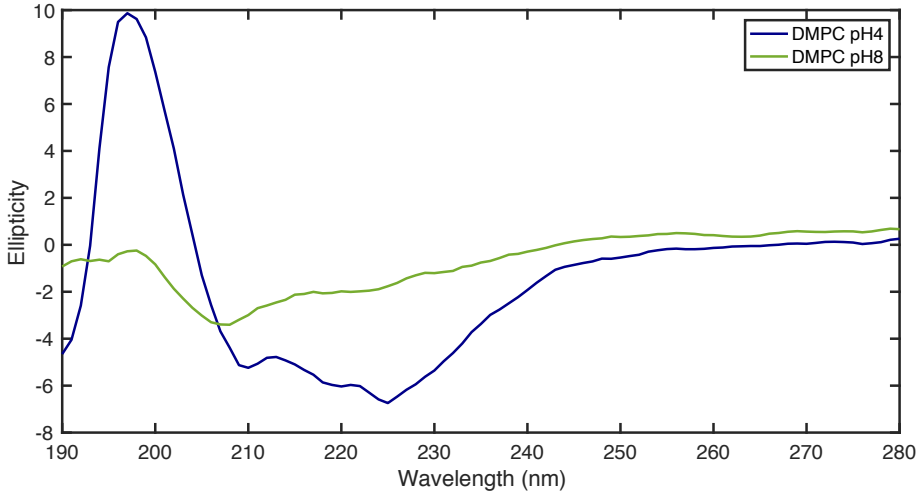

Figure S4. *Circular Dichroism results for pHLIP and DMPC vesicles in MOPS at pH 4 (blue) and pH 8 (green).*

S3. FTIR experiments.

FTIR spectra, given in **Figure S5**, were collected at 1 cm^{-1} resolution at room temperature using a Bruker Vertex 70 spectrometer. The samples were prepared as described in the previous section and were held between two CaF_2 windows with a 50 µm PTFE spacer. The spectra corresponding to the singly labeled peptides are not given as the isotope peaks were not resolved.

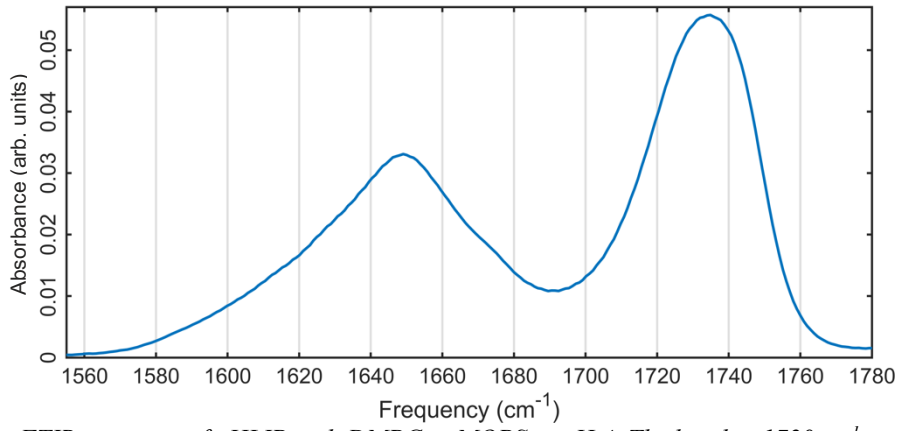

Figure S5. *Top: FTIR spectrum of pHLIP with DMPC in MOPS at pH 4. The band at 1720cm^{-1} corresponds to the ester C=O of the DMPC head group, and the band centered around 1650cm^{-1} is the amide I region.*

The key feature is the alpha helix peak centered at 1650 cm^{-1} and the lack of features between 1555 and 1610 cm^{-1}, which is the region we expect to see deprotonated carboxylate sidechain absorption. **Figure S5** features the FTIR spectrum after subtraction of a solvent (100mM MOPS in D2O) background.

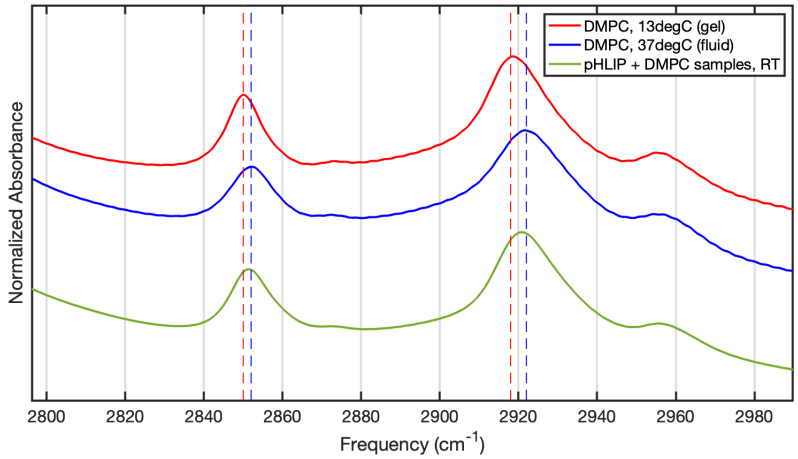

Figure S6. *FTIR spectrum of the asymmetric CH stretching region of gel-phase DMPC at 13°C (top, red), fluid-phase DMPC at 37°C (middle, blue), and DMPC with pHLIP inserted (bottom, green). Vertical dashed lines indicate the frequency$_{max}$ for the two control cases (red representing gel; blue representing fluid) for better visual comparison with experimental pHLIP samples.*

Using the CH asymmetric stretching features of the FTIR spectrum, we determine that these vesicles are in the fluid phase under our experimental conditions. This determination was made from the CH stretch of the FTIR spectrum shown in **Figure S6**, indicated by two peaks near 2850 and 2920 cm^{-1}, respectively, which exhibits a blue shift upon transition to the fluid phase (3). Control spectra of fluid DMPC at 37°C and gel DMPC at 10°C have been included on the same axes for comparative purposes.

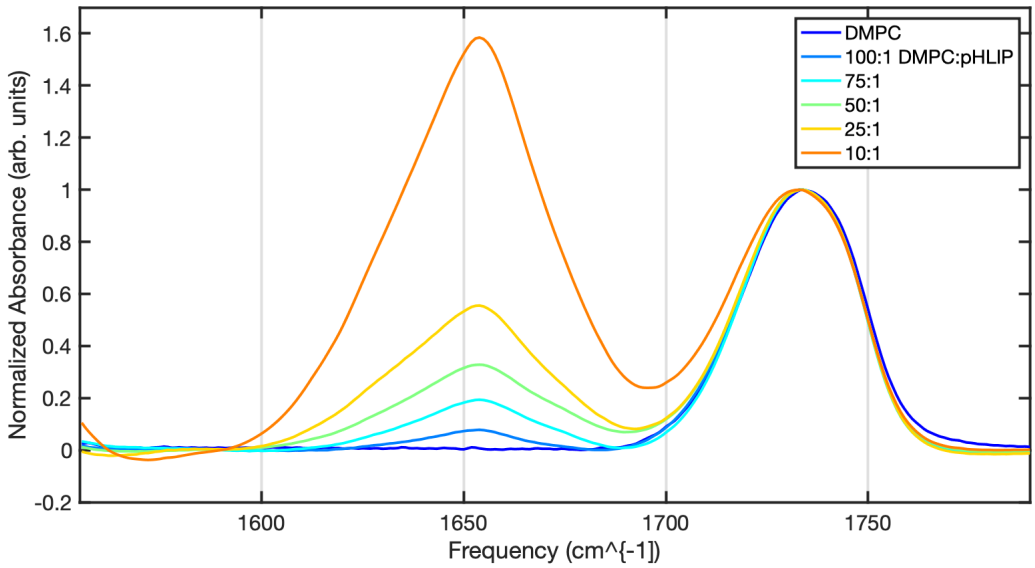

Figure S7*. Concentration-dependent FTIR of pHLIP in DMPC. Peaks are normalized to the maximum intensity of the ester C=O stretch (1730cm^{-1}).*

To rule out the possibility of aggregation, we performed concentration-dependent studies of pHLIP in DMPC, given in **Figure S7**. Protein aggregation is detectable by FTIR as a sharp peak

around 1610 cm^{-1}. No aggregation is detected at the 50:1 DMPC:pHLIP ratio reported here, and there are no observed changes in the amide I lineshape upon changing pHLIP concentration. Thus, aggregates are not present these pHLIP samples, however, these spectra cannot rule out the possibility of peptide-peptide interactions.

S4. 2D IR experiments.

Two-dimensional IR experiments were performed in the time domain using an in-house spectrometer previously described by Edington et. al. (4). Spectra were collected using perpendicular polarization with a population time (T_2) of 500 fs and scanned coherence times (t_1) up to 3 ps in 7 fs steps. Four-frame phase cycling was used to remove scatter. Each spectrum was averaged for 11,200,000 laser shots (approx. 8 hours). Diagonal "slices" were taken +7 cm^{-1} from the diagonal axis for comparison with analogous 2D and MD data. All 2D IR spectra and diagonal slices are normalized to the maximum intensity of the amide-I peak. Diagonal slices, including the main amide I band, are shown in **Figure S8**, where we observe the similarity in lineshape between the unlabeled and each of the labeled samples. It should be noted that in **Figure 5**, a Gaussian fit correspondent to the main band has been subtracted from each spectrum to isolate the isotope region and remove nonzero baseline features.

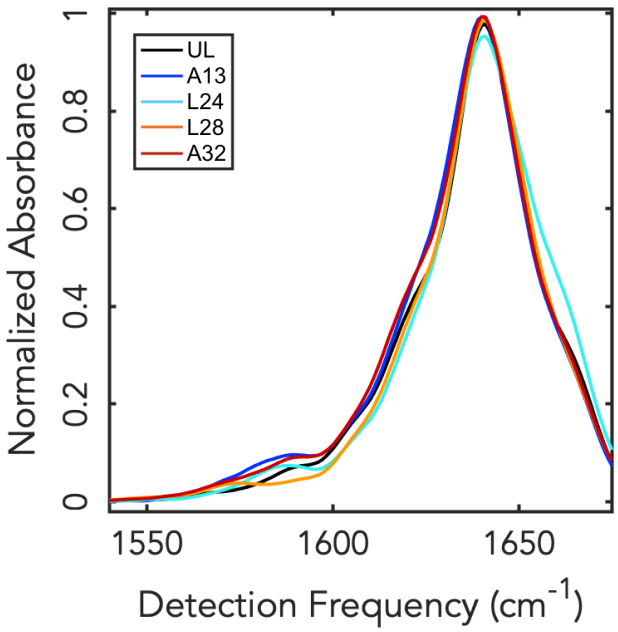

Figure S8. *Diagonal cuts of experimental 2D IR spectra of pHLIP with DMPC in MOPS, pH 4 for the unlabeled and for each isotope labeled peptide. The main band is centered around 1640cm-1.*

S5. Molecular Dynamics Simulations

Molecular dynamics (MD) simulations were carried out using GROMACS 5.1.2 (5). Topologies were generated using CHARMM-GUI as a 9 nm cubic box containing a DMPC bilayer of 64 DMPC molecules per leaflet with an inserted pHLIP as an idealized alpha helix, and solvated with TIP3P water molecules (6–12). Structures were equilibrated in six sequential steps. Trajectories were collected for 10 ns at 300K and 1 atm, storing snapshots every 20 fs for IR calculations and other analysis. Hydrogen bonding (H-bond) analysis was performed using the default hydrogen

bond tool in GROMACS (gmx hbond) to calculate H-bond between the backbone C=O oxygen of each isotope labeled site with water as well as with other peptide atoms. RDF functions were computed using the RDF analysis tool in GROMACS for each labeled site.

a. Spectral Calculations

Spectral calculations used the electrostatic map published by Reppert and Tokmakoff using charges defined by the CHARMM27 force field (13). These frequency maps relate electrostatic potential, electric field, and gradient from classical MD simulations to generate matrix elements for an amide I Frenkel-type Hamiltonian (14). These Hamiltonians were calculated over a 1-ns segment of the trajectory, then diagonalized and propagated using the Trotter formula to compute the linear response function according to methods developed by Thomas la Cour Jansen (15–19). Solutions were then Fourier transformed to generate the frequency-domain spectrum. For 2D IR spectra, the waiting time was set to 0 fs and anharmonicity was defined to be -16 cm^{-1}. The same vibrational Hamiltonians were used to generate the third-order response function and subsequent frequency-domain 2D IR spectra for perpendicular polarization conditions.

S6. Additional MD data

a. Isotope-labeled spectra

Computed spectra of the selected isotope sites are given in **Figure S1** (See Section S1).

b. Main band diagonals

Figure S9 shows the diagonal slices of each of the main band diagonals taken at a +7 cm^{-1} offset from the main diagonal in the 2D plots. Solid lines correspond to experimental data, and dashed lines are the simulated spectra. The bands are conserved in the presence of isotope labels, indicating the structure of the peptide is not perturbed. Additionally, there is agreement between experiment and simulation in terms of line shape and peak frequency. Qualitatively, we see differences in linewidth between experiment and simulation. Possible causes for this disparity have been discussed in the main text (Discussion section) and is further detailed below (**Section S7**).

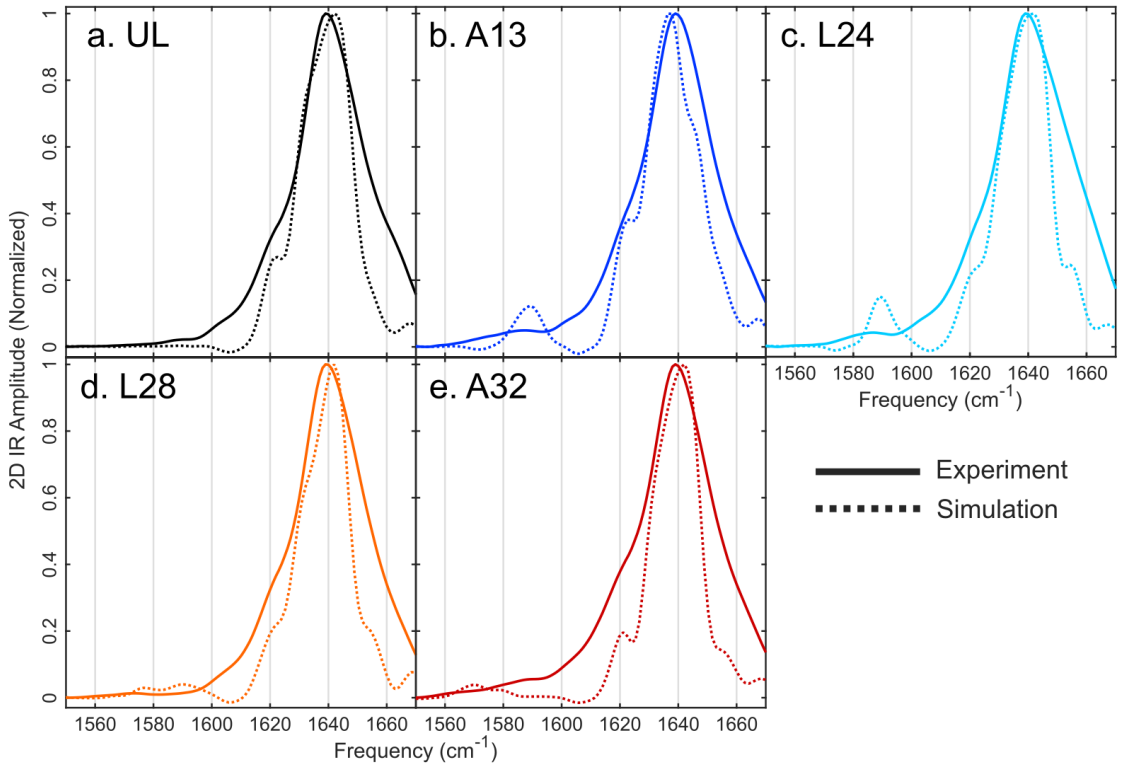

Figure S9. *Diagonal cuts of simulated 2D IR spectra of pHLIP (helix) with DMPC in water. Solid lines are experimental spectra and dashed lines are simulations. The main amide I band is centered around 1640 cm^{-1}, with the additional isotope peak showing up between 1560 and 1610 cm^{-1}.*

S7. Studies of Charge Effects on Spectral Predictions

To trace the origin of the narrowed peaks in the simulated data, we ran several additional spectral calculations on the original trajectory with altered electrostatics, modifying the topology to set the charges on certain molecule types to zero in the spectral calculations (note that coordinates are from the original trajectory). A 5 ns segment of each trajectory was analyzed. In total, we ran 5 different calculations:

1. pHLIP in a DMPC bilayer with standard CHARMM36 charges.
2. pHLIP in DMPC with the water charges set to 0.
3. pHLIP in DMPC with the lipid charges set to 0.
4. pHLIP in water with standard TIP3P charges.
5. pHLIP in water with the water charges set to 0.

Figure S10 summarizes the results of calculating an IR spectrum for each simulation, which demonstrates a lineshape dependence on the assigned charge of the water molecule. The results are further compared in **Figure S11**.

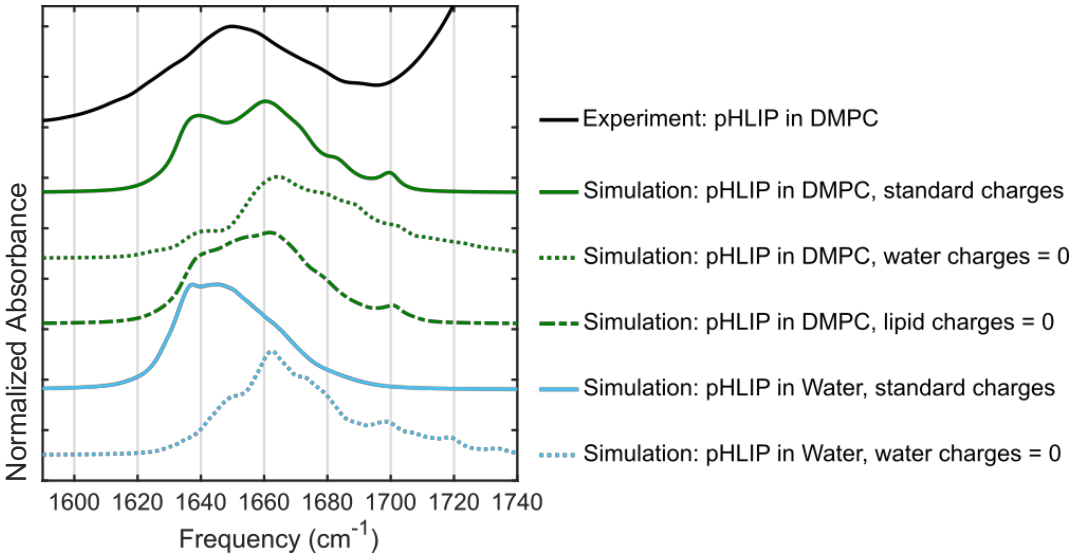

Figure S10. *Computed spectra from MD trajectories using altered electrostatics.*

We observe agreement between pHLIP/DMPC (standard charges) and experiment as well as between pHLIP/water (standard charges) and experiment. However, a key comparison is between pHLIP/DMPC (water = 0) and pHLIP/water (water = 0). While one of these simulations contains lipids and the other is effectively in vacuum, the spectra (**Figure S11**, left) have the same frequency and lineshape, indicating that the electrostatic environment is independent of the lipids.

Similarly, we see negligible changes in the spectrum in the presence of lipids between the calculated spectrum with standard lipid charges versus the spectrum calculated for zero lipid charges (**Figure S11**, right).

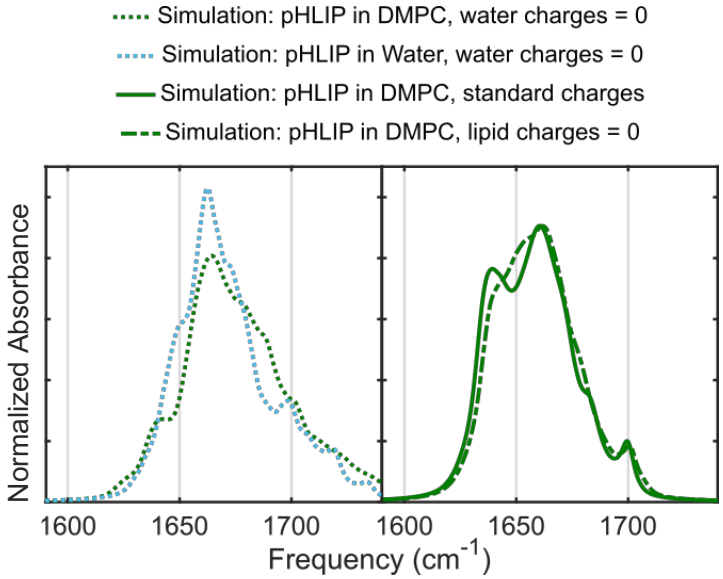

Figure S11. *Computed spectra with altered atomic charges.*

These observations support the hypothesis that the electrostatic maps used in these calculations do not accurately capture the lipid electrostatics, forcing a more homogeneous environment than in the actual system; thus, we attribute this as the source of the narrow peaks in the simulation.

a. Site frequencies: water electrostatics

To further support the claim that the residues within the lipid experience an artificially homogeneous environment, we analyzed the site-specific frequency for each residue throughout the simulation. The plots in **Figure S12** and **Figure S13** contain a histogram for each residue's frequency throughout the simulation, which is extracted from the diagonal elements of the Hamiltonian for each simulation frame.

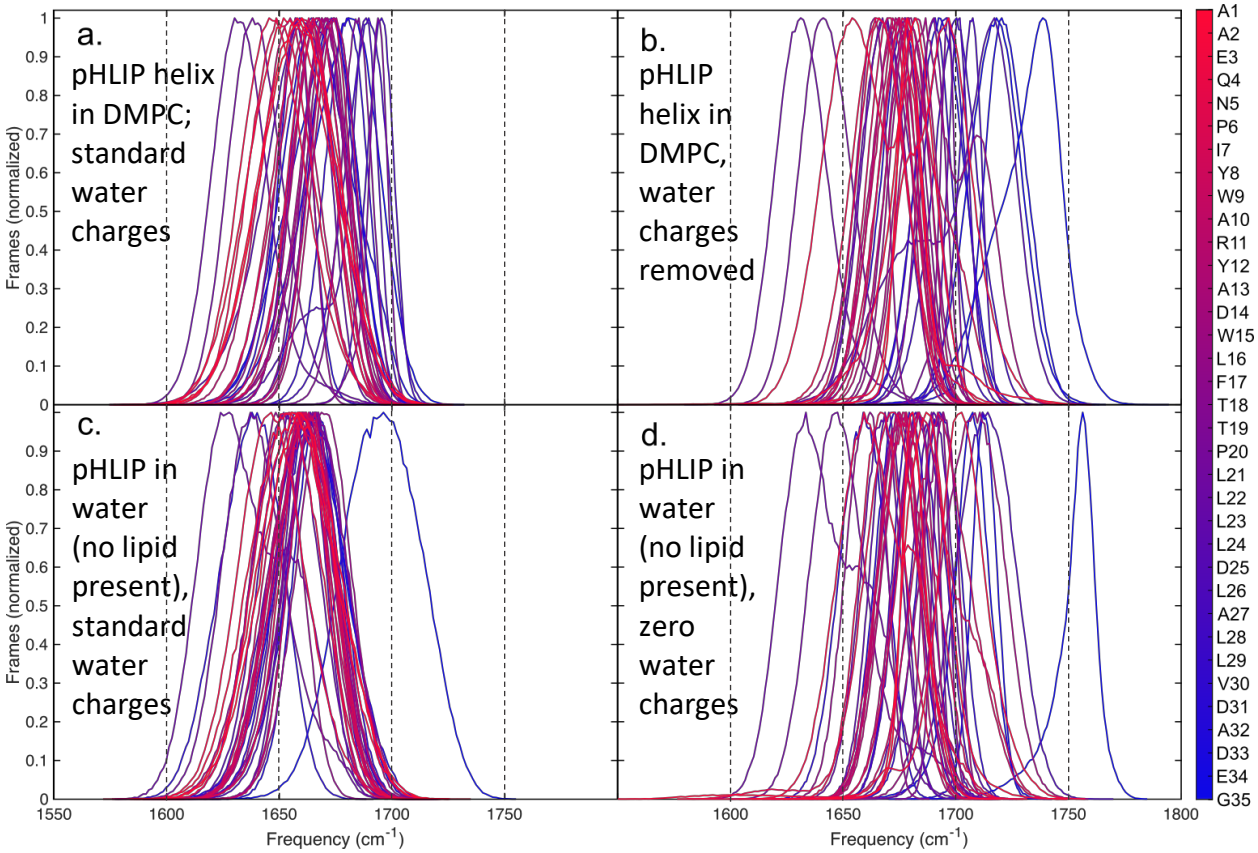

***Figure S12**. Site energy histograms for varied electrostatics simulations. a) pHLIP in DMPC, standard charges; b) pHLIP in DMPC, water charges = 0; c) pHLIP helix in water without DMPC present, standard charges; d) pHLIP helix in water without DMPC present, water charges = 0.*

In the simulations where the water charges have been removed, we see a broader range of frequencies from residue to residue, but each individual histogram is narrower than its counterpart with standard water charges. This indicates that the local environment is more homogeneous without water electrostatics than with (including in the presence of lipid charges), which further supports the initial hypothesis.

b. Site frequencies: lipid electrostatics

Figure S13 highlights the difference in the effect of water on the site frequencies versus the effect of lipid electrostatics.

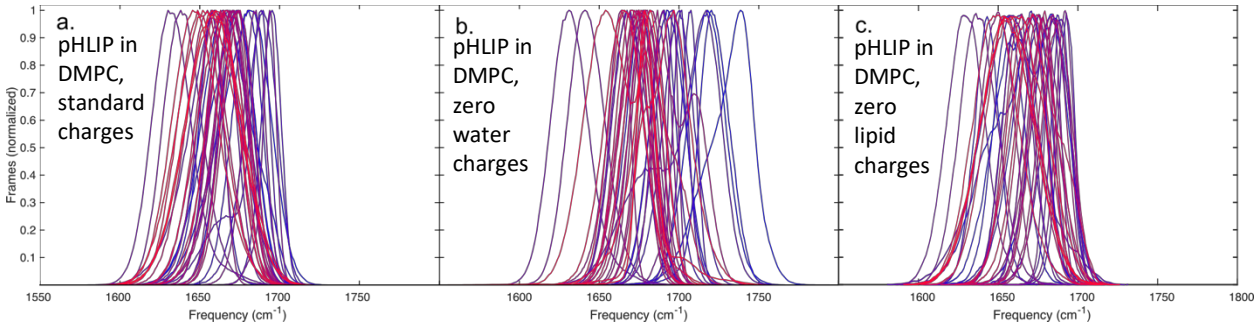

Figure S13. Site energy histograms for varied electrostatic simulations of pHLIP in DMPC bilayer. a) pHLIP in DMPC, standard charges; b) pHLIP in DMPC, water charges =0; c) pHLIP in DMPC, lipid charges = 0.

As expected from the spectral calculations (**Figure S12**), the site histograms show negligible discrepancy between the simulations with and without the lipid charges "turned on." Removing the water charges has a pronounced effect on the frequency distribution.

SUPPORTING REFERENCES

1. Holzwarth, G., and P. Doty. 1965. The Ultraviolet Circular Dichroism of Polypeptides. *J. Am. Chem. Soc*. 87:218-228.
2. Venyaminov, S.Y., I.A. Baikalov, Z.M. Shen, C.S.C. Wu, and J.T. Yang. 1993. Circular Dichroic Analysis of Denatured Proteins: Inclusion of Denatured Proteins in the Reference Set. *Anal. Biochem.* 214:17–24.
3. Lewis, R.N.A.H., and R.N. McElhaney. 2013. Membrane lipid phase transitions and phase organization studied by Fourier transform infrared spectroscopy. *BBA - Biomembr.* 1828:2347–2358.
4. Edington, S.C., A. Gonzalez, T.R. Middendorf, D.B. Halling, R.W. Aldrich, and C.R. Baiz. 2018. Coordination to lanthanide ions distorts binding site conformation in calmodulin. *Proc. Natl. Acad. Sci. USA*. 115:E3126–E3134.
5. Abraham, M.J., T. Murtola, R. Schulz, S. Páll, J.C. Smith, B. Hess, and E. Lindahl. 2015. GROMACS: High performance molecular simulations through multi-level parallelism from laptops to supercomputers. *SoftwareX.* 1–2:19–25.
6. Jo, S., T. Kim, V.G. Iyer, and W. Im. 2008. CHARMM-GUI: A web-based graphical user interface for CHARMM. *J. Comput. Chem.* 29:1859–1865.
7. Brooks, B.R., C.L. Brooks, A.D. Mackerell, L. Nilsson, R.J. Petrella, B. Roux, Y. Won, G. Archontis, C. Bartels, S. Boresch, A. Caflisch, L. Caves, Q. Cui, A.R. Dinner, M. Feig, S. Fischer, J. Gao, M. Hodoscek, W. Im, K. Kuczera, T. Lazaridis, J. Ma, V. Ovchinnikov, E. Paci, R.W. Pastor, C.B. Post, J.Z. Pu, M. Schaefer, B. Tidor, R.M. Venable, H.L. Woodcock, X. Wu, W. Yang, D.M. York, and M. Karplus. 2009. CHARMM: The biomolecular simulation program. *J. Comput. Chem.* 30:1545–1614.
8. Lee, J., X. Cheng, J.M. Swails, M.S. Yeom, P.K. Eastman, J.A. Lemkul, S. Wei, J. Buckner, J.C. Jeong, Y. Qi, S. Jo, V.S. Pande, D.A. Case, C.L. Brooks, A.D. MacKerell, J.B. Klauda, and W. Im. 2016. CHARMM-GUI Input Generator for NAMD, GROMACS, AMBER, OpenMM, and CHARMM/OpenMM Simulations Using the CHARMM36 Additive Force Field. *J. Chem. Theory Comput.* 12:405–413.
9. Jo, S., X. Cheng, S.M. Islam, L. Huang, H. Rui, A. Zhu, H.S. Lee, Y. Qi, W. Han, K. Vanommeslaeghe, A.D. MacKerell, B. Roux, and W. Im. 2014. CHARMM-GUI PDB Manipulator for Advanced Modeling and Simulations of Proteins Containing Nonstandard Residues. *Adv. Protein Chem. Struct. Biol.* 96:235–265.
10. Jo, S., J.B. Lim, J.B. Klauda, and W. Im. 2009. CHARMM-GUI Membrane Builder for Mixed Bilayers and Its Application to Yeast Membranes. *Biophys. J.* 97:50–58.
11. Klauda, J.B., R.M. Venable, J.A. Freites, J.W. O'Connor, D.J. Tobias, C. Mondragon-Ramirez, I. Vorobyov, A.D. MacKerell, and R.W. Pastor. 2010. Update of the CHARMM All-Atom Additive Force Field for Lipids: Validation on Six Lipid Types. *J. Phys. Chem. B.* 114:7830–7843.
12. Jorgensen, W.L., J. Chandrasekhar, J.D. Madura, R.W. Impey, and M.L. Klein. 1983. Comparison of simple potential functions for simulating liquid water. *J. Chem. Phys.* 79:926–935.
13. Reppert, M., and A. Tokmakoff. 2013. Electrostatic frequency shifts in amide I vibrational spectra: Direct parameterization against experiment. *J. Chem. Phys.* 138:134116.
14. Reppert, M., and A. Tokmakoff. 2016. Computational Amide I 2D IR Spectroscopy as a Probe of Protein Structure and Dynamics. *Annu. Rev. Phys. Chem.* 67:359–386.
15. Liang, C., M. Louhivuori, S.J. Marrink, T. la Cour Jansen, and J. Knoester. 2013.

Vibrational Spectra of a Mechanosensitive Channel. *J. Phys. Chem. Lett.* 4:448–452.
16. la Cour Jansen, T., and J. Knoester. 2009. Waiting Time Dynamics in Two-Dimensional Infrared Spectroscopy. *Acc. Chem. Res.* 42:1405–1411.
17. Liang, C., and T. la Cour Jansen. 2012. An Efficient N 3 -Scaling Propagation Scheme for Simulating Two-Dimensional Infrared and Visible Spectra. *J. Chem. Theory Comput.* 8:1706–1713.
18. la Cour Jansen, T., and J. Knoester. 2006. Nonadiabatic Effects in the Two-Dimensional Infrared Spectra of Peptides: Application to Alanine Dipeptide. *J. Phys. Chem. B*, 110:22910-22916.
19. la Cour Jansen, T., B.M. Auer, M. Yang, and J.L. Skinner. 2010. Two-dimensional infrared spectroscopy and ultrafast anisotropy decay of water. *J. Chem. Phys.* 132: 224503.